POLITECNICO DI TORINO
Repository ISTITUZIONALE

The Role of Operating Conditions in the Precipitation of Magnesium Hydroxide Hexagonal Platelets Using NaOH Solutions

Original
The Role of Operating Conditions in the Precipitation of Magnesium Hydroxide Hexagonal Platelets Using NaOH Solutions / Romano, S., Trespi, S., Achermann, R., Battaglia, G., Raponi, A., Marchisio, D., Mazzotti, M., Micale, G., Cipollina, A.. - In: CRYSTAL GROWTH & DESIGN. - ISSN 1528-7483. - 23:9(2023), pp. 6491-6505. [10.1021/acs.cgd.3c00462]

Availability:
This version is available at: 11583/2982495 since: 2023-09-26T19:42:11Z

Publisher:
American Chemical Society

Published
DOI:10.1021/acs.cgd.3c00462

Terms of use:

This article is made available under terms and conditions as specified in the corresponding bibliographic description in the repository

Publisher copyright

(Article begins on next page)

27 November 2026

CRYSTAL GROWTH & DESIGN

pubs.acs.org/crystal

Article

The Role of Operating Conditions in the Precipitation of Magnesium Hydroxide Hexagonal Platelets Using NaOH Solutions

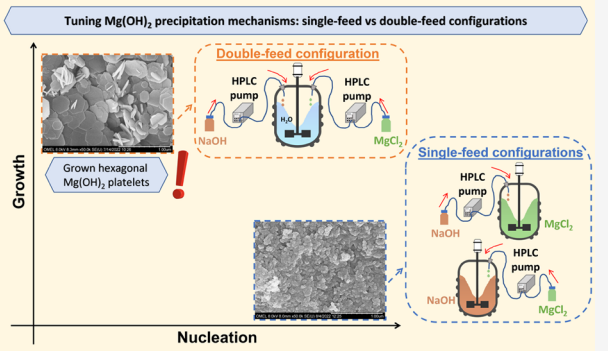
Salvatore Romano, Silvio Trespi, Ramona Achermann, Giuseppe Battaglia,* Antonello Raponi, Daniele Marchisio, Marco Mazzotti, Giorgio Micale, and Andrea Cipollina

Cite This: https://doi.org/10.1021/acs.cgd.3c00462

Read Online

ACCESS | Metrics & More | Article Recommendations | Supporting Information

ABSTRACT: Magnesium hydroxide, $Mg(OH)_2$, is an inorganic compound extensively employed in several industrial sectors. Nowadays, it is mostly produced from magnesium-rich minerals. Nevertheless, magnesium-rich solutions, such as natural and industrial brines, could prove to be a great treasure. In this work, synthetic magnesium chloride and sodium hydroxide (NaOH) solutions were used to recover $Mg(OH)_2$ by reactive crystallization. A detailed experimental campaign was conducted aiming at producing grown $Mg(OH)_2$ hexagonal platelets. Experiments were carried out in a stirred tank crystallizer operated in single- and double-feed configurations. In the single-feed configuration, globular and nanoflakes primary particles were obtained, as always reported in the literature when NaOH is used as a precipitant. However, these products are not complying with flame-retardant applications that require large hexagonal $Mg(OH)_2$ platelets. This work suggests an effective precipitation strategy to favor crystal growth while, at the same time, limiting the nucleation mechanism. The double-feed configuration allowed the synthesis of grown $Mg(OH)_2$ hexagonal platelets. The influence of reactant flow rates, reactant concentrations, and reaction temperature was analyzed. Scanning electron microscopy (SEM) pictures were also taken to investigate the morphology of $Mg(OH)_2$ crystals. The proposed precipitation strategy paves the road to satisfy flame-retardant market requirements.



1. INTRODUCTION

In 2011, the European Union (EU) published the first list of high-supply risk "Critical Raw Materials", CRMs,[1] for the economy and social development of the EU. Magnesium, included among CRMs, is a shiny gray metal. EU imports more than 93% of magnesium from China. To tackle the EU mineral resource scarcity, alternative sources must be identified. In this context, the sea salt manufacturing process in saltworks generates a byproduct waste stream, called brine or bittern. Saltworks bitterns are characterized by a very high magnesium concentration reaching values up to 60 g/L, about 40 times higher than that in seawater (1.1−1.7 g/L).[2] The high magnesium content makes bitterns excellent candidates for the recovery of this element, turning waste into a treasure.

A winning strategy is to extract magnesium in the form of magnesium hydroxide, $Mg(OH)_2$, via reactive crystallization.[3,4] Magnesium hydroxide is a white and odorless compound extensively employed as (i) an excipient for pharmaceutical and nutraceutical products; (ii) an acidic waste neutralizer thanks to its adsorptive and coagulative properties, (iii) a precursor for magnesium oxide and magnesium carbonate production, and (iv) a smoke-suppressing flame-retardant agent in composite polymeric materials.[5,6] Depending on the industrial application, $Mg(OH)_2$ products must fulfill specific requirements. As an example, flame-retardant applications require $Mg(OH)_2$ hexagonal platelets characterized by an average particle size of ∼0.5 to 1.5 μm and a specific surface area of less than 10 m^2/g.[7] These characteristics have been typically achieved by adopting solvo/hydrothermal and microwave heating treatments.[8,9] Hydrothermal synthesis, however, requires relatively long reaction times (from 6 to 24 h or more) and high temperatures (up to 200 °C).[10] Several studies have dealt with the possibility to synthesize $Mg(OH)_2$ hexagonal platelets via reactive crystallization using aqueous ammonia solution, NH_4OH, or sodium hydroxide solutions.[11−14] $Mg(OH)_2$ hexagonal platelets have been synthesized using NH_4OH, while, to the best of the authors' knowledge, globular or flakes nano-primary particles have been reported employing only NaOH solutions.[15,16] However, low Mg^{2+} conversions are typically attained when using NH_4OH solutions. Further, the presence of ammonium ions (byproducts) makes the suspensions dangerous especially if

Received: April 16, 2023
Revised: July 25, 2023

Downloaded via POLITECNICO DI TORINO on September 1, 2023 at 08:18:50 (UTC).
See https://pubs.acs.org/sharingguidelines for options on how to legitimately share published articles.

© XXXX The Authors. Published by American Chemical Society

these are employed in electrolytic processes.[17] Conversely, NaOH solutions guarantee a 100% Mg^{2+} conversion with no dangerous byproducts.[2]

When using NaOH solutions, the $Mg(OH)_2$ precipitation process has been reported to be characterized by very fast nucleation kinetics, considerably higher than growth kinetics even at low reactant concentrations of about 2 mM.[18]

In the process, reactants' mixing is the rate-determining step affecting the final produced particle features.[19,20] Battaglia et al.[21] investigated the influence of mixing on $Mg(OH)_2$ particles precipitated from synthetic 1 M $MgCl_2$ and 2 M NaOH solutions employing two T-mixers. An analytical method was followed to characterize $Mg(OH)_2$ particle assembly state by treating $Mg(OH)_2$ suspensions with ultrasound and adding the poly(acrylic acid, sodium salt) as a dispersant. Tai et al.[22] synthesized nanosized round and disk-shaped $Mg(OH)_2$ particles in a spinning disk reactor using 0.2−0.92 M $MgCl_2$ and 0.4−1.84 M NaOH solutions. The authors analyzed the influence of rotation speed, reactant flow rates, and concentrations on the produced $Mg(OH)_2$ particles. Synthesized $Mg(OH)_2$ powders were dispersed in water with the aid of a sonicator also adding poly(acrylic acid, sodium salt) and sodium hexametaphosphate as dispersants. Shen et al.[23] explored the $Mg(OH)_2$ precipitation in a novel impinging stream-rotating packed bed reactor employing 0.25−1.25 M $MgCl_2$ and 0.5−2.5 M NaOH solutions. Particles were analyzed after dispersion in distilled water by sonication adding only a sodium hexametaphosphate solution as a dispersant. Ren et al.[7] synthesized $Mg(OH)_2$ particles from 1 M $MgCl_2$ and 2 M NaOH solutions in a T-type microchannel reactor at 70 °C.

$Mg(OH)_2$ precipitation was also investigated in stirred tank reactors. Mullin et al.[24] precipitated $Mg(OH)_2$ by mixing $MgCl_2$ and NaOH solutions in a single-feed batch reactor. The authors studied the influence of different reactant concentrations (Mg^{2+} = 12.5, 25, and 50 mM) and stirring speeds (250, 500, and 700 rpm). Wu et al.[25] performed $Mg(OH)_2$ precipitation using $MgCl_2$ and NaOH in a single-feed semi-batch reactor. The authors also treated the samples by hydrothermal treatment in the presence of 1 g/L of calcium chloride to increase the particle size and improve their morphology.

Overall, in all of the above-discussed studies, with the exception of the hydrothermal case, only $Mg(OH)_2$ globular nanometric primary particles (50−200 nm) were always identified.

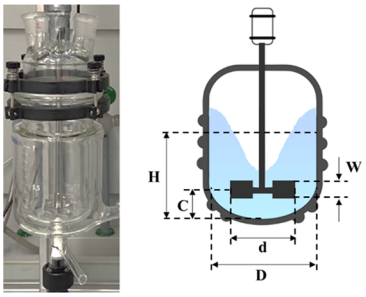
To favor crystal growth in the precipitation process of sparingly soluble compounds, Stavek et al.[26] conducted the precipitation of silver halide compounds in a stirred beaker, feeding the reagents using controlled double jets. Song et al.[16] tried to synthesize hexagonal magnesium hydroxide crystals in a single- and double-feed batch reactor under vigorous stirring. Highly concentrated $MgCl_2$ solutions (2−4.5 M) and stoichiometric NaOH solution were added to a NaCl solution (2−3.5 M). Micro-sized ball-like aggregate/agglomerates particles were identified. Henrist et al.[11] also performed $Mg(OH)_2$ precipitation tests in a double-feed mode system exploring the influence of (i) alkaline solution types, i.e., NaOH or NH_4OH; (ii) types of counterions, i.e., Cl^-, NO_3^- or SO_4^{2-}; and (iii) reaction temperature. Globular ∼300 nm cauliflower particles were precipitated from NaOH solutions at 60 °C, while ∼360 nm platelet-shaped crystals were obtained with NH_4OH. No $Mg(OH)_2$ hexagonal platelets were achieved in both studies.

This short literature review clearly highlights that despite several attempts, no hexagonal platelet $Mg(OH)_2$ crystals precipitated from $MgCl_2$ solutions using NaOH have ever been reported.

The present work aims at filling this gap by thoroughly analyzing the magnesium hydroxide precipitation process in single- and double-feed semi-batch crystallizers. Several operating conditions were explored, aiming at triggering crystal growth using NaOH solutions. These $Mg(OH)_2$ particles would be of high interest in view of recovering $Mg(OH)_2$ from natural wastes as saltworks bitterns. In the experimental campaign, synthetic $MgCl_2$ and NaOH solutions were employed and the effect of reactant flow rates, reactant concentrations, and reaction temperature was investigated. Synthesized $Mg(OH)_2$ products were characterized in terms of size, morphology, and surface area properties. For the first time in the literature, $Mg(OH)_2$ platelet crystals were obtained using relatively concentrated $MgCl_2$ and NaOH solutions without any dispersant addition or modification treatment. This result was achieved by accurately controlling the operating conditions in a double-feed semi-batch stirred reactor. The relevance of the here presented experimental campaign does not only apply to the case of the recovery of $Mg(OH)_2$ from brines. The accurate control of the supersaturation level in a double-feed semi-batch stirred reactor, marked in the present work, can be extended to the precipitation of sparingly soluble compounds, whose precipitation processes are characterized by very fast kinetics.

2. MATERIALS AND METHODS

2.1. Experimental Setup. $Mg(OH)_2$ precipitation tests were carried out in a jacketed glass unbaffled stirred tank reactor, depicted in Figure 1a. An unbaffled configuration was chosen to prevent any



(c)

Proportions	Ratio value
H/D	1
d/D	1/2
C/H	1/3
W/d	1/5

Figure 1. (a) Picture of the employed crystallizer; (b) schematic representation of the employed $Mg(OH)_2$ unbaffled stirred tank crystallizer, and (c) geometrical proportions reflecting the standard geometry of the stirred tank.

undesirable secondary phenomena, e.g., secondary nucleation events at the baffles.[27,28] Theoretical and empirical correlations have been proposed in the literature to estimate mixing times in unbaffled stirred tanks, adopting specific geometrical reactor configurations, referred to as the standard geometry.[29,30] In the present experimental campaign, the adopted jacketed reactor, whose schematic representation and geometry proportions are reported in Figure 1b,c, had a 0.100 m diameter, *D*, with a round bottom. A six-blade Rushton turbine of 0.050 m diameter, *d*, and 0.010 m blade height, *W*, was employed and placed at 0.033 m, *C*, from the bottom of the tank. In all experiments, the liquid height, *H*, at the end of the test was 0.100 m, equivalent to a volume of 0.785 L. All geometry features were chosen to be complying with a typical standard geometry investigated in the literature.[29]

To comply with the standard geometry proportions, experiments were started with an initial volume of 0.685 L, equivalent to a liquid height of 0.087 m. After adding a volume of reactants of 0.100 L, the total volume increased by less than 15%, reaching the standard 0.100 m

https://doi.org/10.1021/acs.cgd.3c00462
Cryst. Growth Des. XXXX, XXX, XXX−XXX

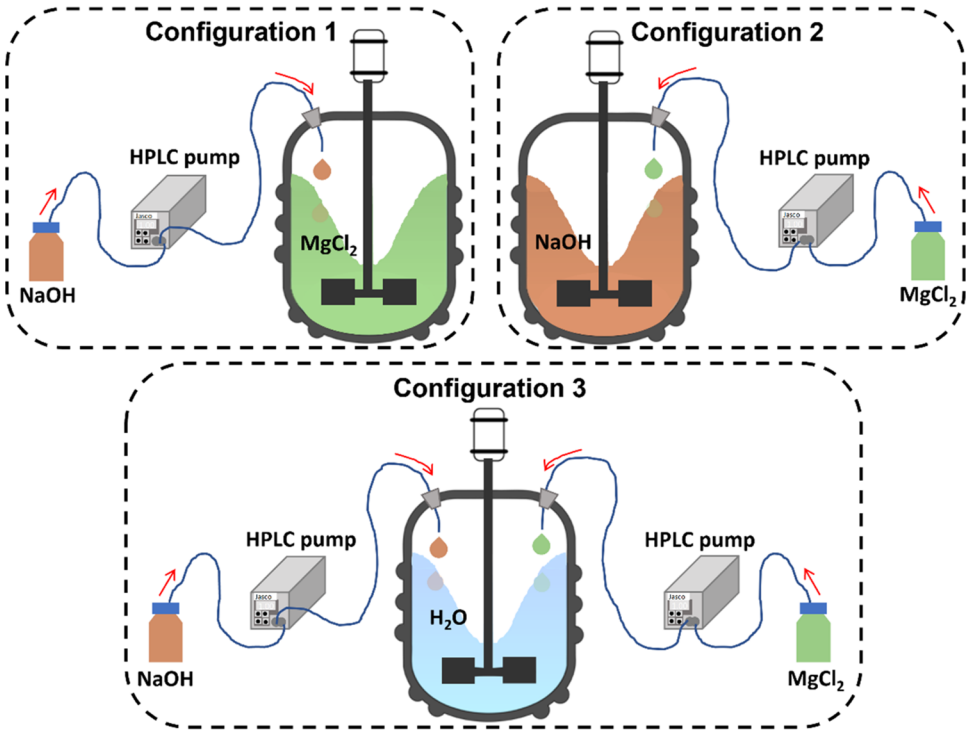


Figure 2. Schematic representation of the three employed configurations. High-performance liquid chromatography (HPLC) pumps were used to feed the solutions.

Table 1. Operating Conditions Adopted during Single- and Double-Feed Experiments[a]

setup config.	case	$MgCl_2$ concentration [M]	NaOH concentration [M]	flow rate (Q) [mL/min]	feeding time (t_f) [min]	temperature [°C]
1	1	0.036 ± 0.002	0.500 ± 0.025	1.00 ± 0.05	100	25 ± 1
	1.f1	0.036 ± 0.002	0.500 ± 0.025	0.500 ± 0.025	200	25 ± 1
2	2	0.250 ± 0.013	0.072 ± 0.004	1.00 ± 0.05	100	25 ± 1
	2.f1	0.250 ± 0.013	0.072 ± 0.004	0.500 ± 0.025	200	25 ± 1
3	3	0.500 ± 0.025	1.00 ± 0.05	0.500 ± 0.025	100	25 ± 1
	3.f1	0.500 ± 0.025	1.00 ± 0.05	0.250 ± 0.013	200	25 ± 1
	3.f2	0.500 ± 0.025	1.00 ± 0.05	1.00 ± 0.05	50	25 ± 1
	3.f3	0.500 ± 0.025	1.00 ± 0.05	5.00 ± 0.25	10	25 ± 1
	3.f4	0.500 ± 0.025	1.00 ± 0.05	7.50 ± 0.40	6.5	25 ± 1
	3.c1	0.125 ± 0.006	0.250 ± 0.013	0.500 ± 0.025	100	25 ± 1
	3.c2	0.250 ± 0.013	0.500 ± 0.025	0.500 ± 0.025	100	25 ± 1
	3.c3	1.00 ± 0.05	2.00 ± 0.10	0.500 ± 0.025	100	25 ± 1
	3.t1	0.500 ± 0.025	1.00 ± 0.05	0.500 ± 0.025	100	6 ± 1
	3.t2	0.500 ± 0.025	1.00 ± 0.05	0.500 ± 0.025	100	60 ± 1

[a]Quantity uncertainties were estimated by combining the dispersion observed between different trials (reproducibility error) and instrument uncertainties.

level. This strategy allowed the ratio H/D to be roughly maintained during all experimental tests. The stirring speed was set equal to 400 rpm to guarantee a good mixing yet avoiding any air bubbles entraining from the vortex. Under the adopted operating conditions, the tip speed and the specific power input were ∼1 m/s[31] and 92 W/m^3,[29] respectively. The mixing time in the adopted stirred reactor was estimated to be about 15 s, following the correlation reported by Scargiali et al.[29]

$Mg(OH)_2$ precipitation tests were conducted following two different semi-batch operating strategies: (i) a single-feed and (ii) a double-feed. In the single-feed mode, a solution volume of 0.100 L of one of the reactants was fed into a 0.685 L solution of the other one; conversely, in the double-feed arrangement, 0.050 L of $MgCl_2$ and NaOH solutions, for a total volume addition of 0.100 L, were pumped into 0.685 L ultrapure water bath. Figure 2 is a schematic representation of the two operating strategies resulting in 3 configurations: (i) Configurations 1 and 2, where either NaOH or $MgCl_2$ solutions were pumped in single-feed arrangement into either $MgCl_2$ or NaOH baths, respectively, and (ii) Configuration 3, where NaOH and $MgCl_2$ solutions were added into the reactor already filled with ultrapure water.

In all tests, magnesium chloride ($MgCl_2$; Sigma-Aldrich BioXtra, ≥99.0%) and sodium hydroxide (NaOH; Sigma-Aldrich puriss. p.a., ACS reagent, $K \leq 0.02\%$, ≥98.0%) pellets were dissolved in ultrapure water (Milli-Q) to prepare the feed solutions. The use of analytical-grade reagents ensured a high purity of the synthesized $Mg(OH)_2$ products. Moreover, $Mg(OH)_2$ always crystallizes in the trigonal $P\bar{3}m1$ space group.

Magnesium and hydroxyl ions concentrations were checked by complex titration with (i) ethylenediaminetetraacetic acid (EDTA), for Mg^{2+}, and (ii) acid−base titration, for OH^-. Reactants solutions were fed drop-wise using high-performance liquid chromatography (HPLC) pumps (JASCO PU-986). Most of the experiments were carried out at

https://doi.org/10.1021/acs.cgd.3c00462
Cryst. Growth Des. XXXX, XXX, XXX−XXX

room temperature. For tests at 6 and 60 °C, the temperature (T) of the reaction environment was kept constant using a Huber Ministat waterbath. This device was equipped with a pumping system to handle the cooling or heating fluid (distilled water) in the plain jacket. All experiments were conducted adopting stoichiometric reactants solutions amount. The solution/suspension pH was monitored offline or inline by a pH probe (Metrohom Profitrode electrode), and its final value was always in the range between 10.4 and 10.6, thus ensuring the complete reagents' conversion.

2.1.1. Test Conditions. Table 1 lists the precipitation tests conducted in single- and double-feed modes. Four tests were carried out in single-feed modes (Configurations 1 and 2) studying the influence of reactants feeding flow rates. Conversely, the effect of different parameters was analyzed in the double-feed mode (Configuration 3), namely: (i) feed solutions flow rates, (ii) feed solutions concentrations, and (iii) reaction temperature. In Table 1, cases are grouped based on the adopted Configuration, i.e., 1, 2, or 3. The reproducibility and repeatability of the experimental data are discussed in the Supporting Information.

A reference case was chosen for each configuration, and additional letters were used to indicate the parameter varied in the tests, i.e., (*c*) reagent concentration, (*t*) temperature, and (*f*) flow rate. After the letters, a number was added to distinguish cases at a fixed parameter. The range of parameters was chosen as follows: (i) reference cases, namely, Cases 1, 2, and 3, were characterized by the same final ∼1.4 g mass of precipitate; (ii) Mg^{2+} concentrations embraced values from that of seawater (∼0.06 M) to real brine (∼1.00 M); (iii) reactant flow rates were typical of lab scale studies; and (iv) the reaction temperature range was identified according to operational limits of the Huber Ministat waterbath device.

2.2. $Mg(OH)_2$ Particle Characterization Strategy. *2.2.1. Particle Size Distributions: Static and Dynamic Light Scattering Techniques.* $Mg(OH)_2$ particle size distributions (PSDs) were measured by static (SLS) and dynamic light scattering (DLS) techniques. All measurements were performed with and without ultrasound treatment (US) and the addition of the dispersant poly(acrylic acid, sodium salt), (PAA, MW1200, Sigma-Aldrich, Inc.), to accurately characterize $Mg(OH)_2$ particles reducing their agglomeration influence.[11,21] At least 5 volume-PSD measurements for each sample were performed.

The SYMPATEC HELOS granulometer (R3 LENS, f = 100 mm, 0.5/0.9−175 μm) was employed to characterize particle sizes in the range of 0.7−175 μm, while the Zetasizer Nano ZS (Malvern Instruments, U.K.) was adopted for particle sizes measurements between 0.010 and 3 μm. The $Mg(OH)_2$ refractive index was set at 1.58.

Specifically:

(1) $Mg(OH)_2$ particles larger than 0.7 μm were characterized using the SYMPATEC HELOS granulometer. This device was equipped with a SUCELL wet dispersion system having a small volume adapter (∼50 mL) provided with a stirrer for sample homogenization. The pump speed was set at 50% following the SUCELL user guide. In the absence of ultrasound treatment and PAA addition, measurements were carried out as follows: (1) the volume adapter was filled with ultrapure water reaching a volume of ∼50 mL; (2) $Mg(OH)_2$ slurry was gradually added until an obscuration between 15 and 20% was reached, corresponding to a solids concentration of about 0.3 g/L. Conversely, when adopting PAA and ultrasound, a different procedure was followed: (1) samples were diluted in ultrapure water until reaching a solid concentration of about 0.3 g/L; (2) the PAA dispersant was added until reaching a concentration of 4.9 g/kg in the diluted suspension; (3) samples were exposed to an ultrasonic bath (Elma Elmasonic S 40 H (220−240 V), ultrasonic frequency of 37 kHz) for 5 min; and (4) the diluted samples were loaded into the small volume adapter (∼50 mL) to perform the analyses.

(2) $Mg(OH)_2$ particles smaller than 1 μm were characterized using the Malvern Zetasizer Nano ZS device. In the absence of ultrasound treatment and PAA addition, measurements were carried out as follows: (1) samples were diluted in ultrapure water until reaching a solid concentration of 0.3 g/L, as suggested by the user guide; (2) the diluted suspension was loaded into a disposable cuvette and the analysis was carried out. Conversely, when adopting PAA and ultrasounds, measurements were conducted as follows: (1) samples were diluted in ultrapure water until reaching a solid concentration of 0.3 g/L; (2) the PAA dispersant was added until reaching a concentration of 4.9 g/kg in the diluted suspension; (3) samples were exposed to an ultrasonic bath (Elma Elmasonic S 40 H 220−240 V, ultrasonic frequency of 37 kHz) for 5 min; and (4) the diluted suspension was loaded into a disposable cuvette and the analysis was carried out.

In all cases, volume PSDs measurements were performed within 10 min after completion of the precipitation tests. For all of the collected volume PSDs, their median diameters, namely, $d(0.5)$, were determined. The $d(0.5)$ is the median diameter that halves the volume distribution, i.e., 50% of the particles lie below and above the $d(0.5)$ value. Average median diameters and their standard deviations (calculated among 5 measurements) are discussed in Section 3, while, for the sake of completeness, average volume PSDs are reported in Appendix A.

The SYMPATEC HELOS granulometer and the Zetasizer Nano ZS are based on static light scattering and dynamic light scattering techniques, respectively. Different PSDs for the same sample can be obtained by adopting the two techniques. In the Supporting Information, the possible results offset is discussed considering PSDs of Case 3 and Case 3.c1.

2.2.2. Morphological Analyses: Scanning Electron Microscopy (SEM) Technique. $Mg(OH)_2$ particle morphology was assessed by scanning electron microscopy (SEM) technique using a Hitachi S-4800 scanning electron microscope. Samples were prepared as follows: (1) $Mg(OH)_2$ suspensions were filtered with a Whatman GF/A glass microfiber filters (pore size of 1.6 μm) using a Büchner system; (2) cakes were washed with ultrapure water (Milli-Q) to remove residual sodium chloride traces (reaction byproducts); (3) cakes were dried in an oven at 120 °C for 24 h; (4) dry cakes were finally crushed with mortar and pestle; and (5) a platinum−palladium alloy coating was applied to make samples conductive. In the Supporting Information, SEM micrographs at different locations of the same sample are provided to demonstrate the relevance of the observations made in Section 3.

2.2.3. Specific Surface Area Analyses: Brunauer−Emmett−Teller (BET) Technique. The specific surface area of $Mg(OH)_2$ particles was determined by Brunauer−Emmett−Teller (BET) analyses (TriStar II Plus, Micromeritics). Samples were prepared following the same procedure as that for SEM analysis (Section 2.2.2). Before BET measurements, solids were degassed in a nitrogen environment for 3 h at 180 °C.

3. RESULTS AND DISCUSSION

In this section, the results of $Mg(OH)_2$ precipitation tests are presented. A preliminary discussion is made regarding the reaction environment conditions attained in the three reactor configurations. To distinguish the nature and origin of different $Mg(OH)_2$ particles, the following nomenclature has been adopted:

- primary particles are single crystals;
- aggregates consist of many primary particles, linked by strong chemical bonds that cannot be broken by neither fluid shear stresses nor sonication;
- agglomerates are made of primary particles, aggregates, or a mixture of the two, bonded together by electrostatic forces. Agglomerates are weaker than aggregates and can be unpacked by physical treatments such as sonication.[32]

3.1. Preliminary Estimation of Supersaturation in Different Reactor Configurations. The driving force of a crystallization process is supersaturation (S), which is related to the actual concentration of a solute in a solution with respect to its solubility value.

https://doi.org/10.1021/acs.cgd.3c00462
Cryst. Growth Des. XXXX, XXX, XXX−XXX

Table 2. Estimation of Supersaturation Levels for the Three Investigated Configurations[a]

setup config.	1		2		3			
case	1		2		3			
	before dilution	after dilution	before dilution	after dilution	before dilution	after dilution (5%)	after dilution (10%)	after dilution (20%)
$MgCl_2$ conc. [M]	0.036		0.250		0.500	7.30×10^{-4}	3.65×10^{-4}	1.82×10^{-4}
NaOH conc. [M]	0.500		0.072		1	14.6×10^{-4}	7.30×10^{-4}	3.65×10^{-4}
activity coeff. ($\gamma_{\pm}$)	0.45		0.35		0.30	0.88	0.91	0.93
supersat. (S)	1.5×10^8		1.0×10^7		2.4×10^9	1.9×10^2	2.5×10^1	2.5×10^0

[a]A reactant drop of 50 μL was assumed to react as soon as it meets the other reagent in single-feed modes (Configurations 1 and 2), while in the double-feed mode, reactants drops were estimated to dilute in a volume equivalent to 5, 10, and 20% of the total volume (0.685 L) before reaction (Configuration 3).

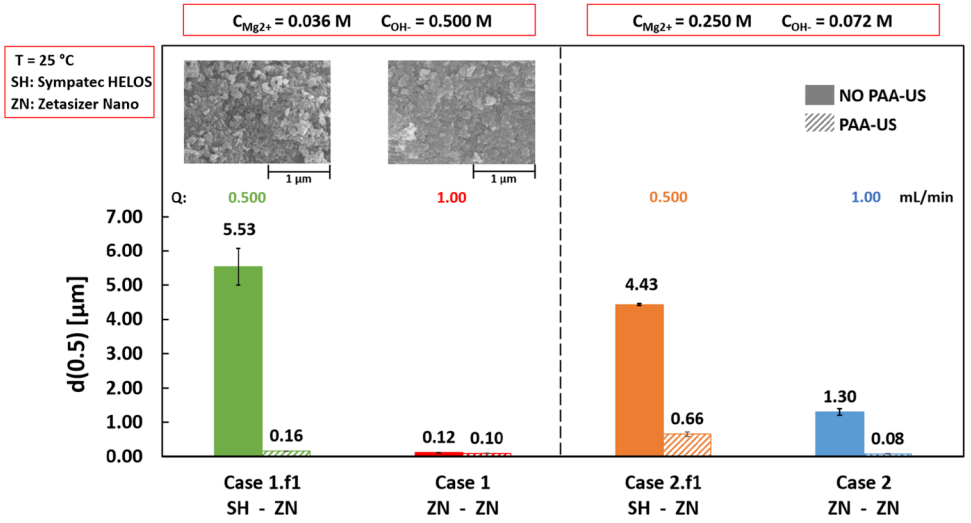


Figure 3. Median diameter $d(0.5)$ values calculated before (solid bars) and after (diagonal stripes bars) PAA-US for single-feed cases. Configuration 1: 0.036 M $MgCl_2$ and 0.500 M NaOH. Configuration 2: 0.250 M $MgCl_2$ and 0.072 M NaOH. The bottom row indicates the employed particle size analyzer: Sympatec HELOS (SH) or Zetasizer Nano (ZN). The upper row reports SEM images.

In the $Mg(OH)_2$ precipitation process, Mg^{2+} ions react with hydroxyl ones (OH^-) provided by an alkaline reactant, i.e., NaOH. The driving force of the process is the supersaturation that is established when the solute concentration exceeds its solubility value. In the present study, supersaturation (S) is expressed in relative form as the difference between the product of ions activity and the solubility product (k_{sp}) divided by k_{sp}, as follows[18]

$$S = \frac{a_{Mg^{2+}} \cdot a_{OH^-}^2 - k_{sp}}{k_{sp}} = \frac{\gamma_{\pm}[Mg^{2+}] \cdot \gamma_{\pm}^2[OH^-]^2 - k_{sp}}{k_{sp}}$$
$$; \; k_{sp} = [Mg^{2+}]_{eq}[OH^-]_{eq}^2 = 5.6 \times 10^{-12} \; [M]^3 \quad (1)$$

where $\gamma_{\pm}$ is the activity coefficient for multicomponent salt solutions that can be calculated by exploiting equations provided by Bromley.[33]

In the present experimental investigation, Mg^{2+} and OH^- ions were added in single- and double-feed modes, as schematically represented in Section 2, see Figure 2. In single-feed mode (Configurations 1 and 2, Figure 2), a drop of one reactant immediately gets in contact with the other reagent present in the liquid volume. Due to the very low $Mg(OH)_2$ solubility, a significant local supersaturation level is reached, inducing the fast $Mg(OH)_2$ precipitation before the complete dilution of the reagent droplet in the whole liquid volume. In this case, nucleation of nanometric particles, prone to aggregate rather than grow, occurs, as largely discussed in the literature.[34]

In the double-feed mode (Configuration 3, see Figure 2) conversely, the two reactants' drops are fed into a water bath. If reactants are added from two opposite sites, as performed in the present work, reactants most likely dilute into the water bath before they meet and react. In this case, lower supersaturation levels can be foreseen with respect to the single-feed mode. On this basis, the possible order of magnitude of the initial supersaturation levels attained at the beginning of the experiments for the investigated configurations was estimated and is reported in Table 2. An instantaneous reaction between reactant drops and solution bath was assumed for the single-feed mode, while a dilution of the reactant drop (volume of drop equal to 0.050 mL) was considered to occur in a volume equivalent to 5, 10, and 20% of the reactor total volume (0.685 L).

In single-feed modes, the initial supersaturation values are expected to be very high (e.g., 10^7–10^8) due to the instantaneous contact between the two reagents see Table 2. Therefore, $Mg(OH)_2$ precipitation will occur immediately at high reactant concentrations. Conversely, lower supersaturation values are expected in double-feed mode, favored by the high dilution factor in the water bath, leading the $Mg(OH)_2$ precipitation to occur in milder conditions (namely, 1.9×10^2, 2.5×10^1, and 2.5×10^0 considering a drop dilution in a volume equivalent to 5, 10, and 20% of the total reactor volume,

https://doi.org/10.1021/acs.cgd.3c00462
Cryst. Growth Des. XXXX, XXX, XXX−XXX

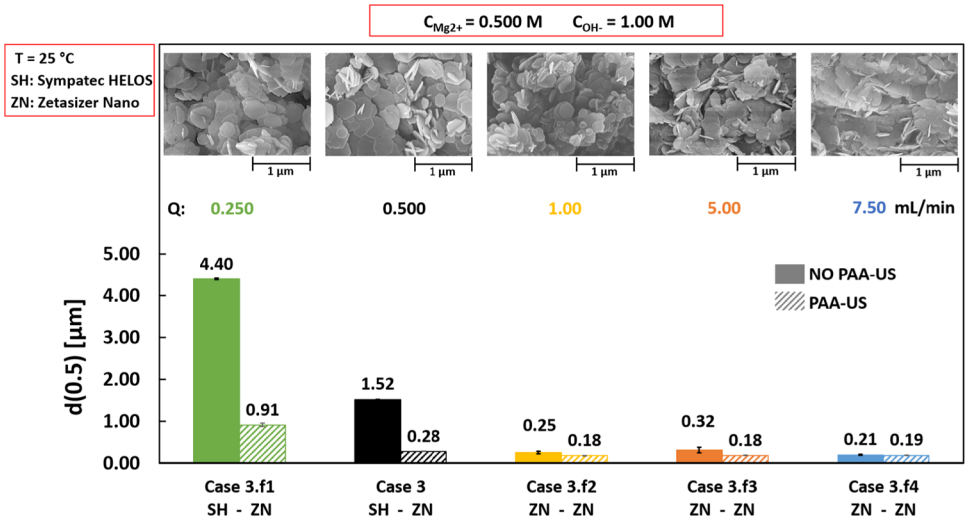


Figure 4. Effect of reagents feed flow rates on median diameter $d(0.5)$ values calculated before (solid bars) and after (diagonal stripes bars) PAA-US. Flow rates of 0.250 mL/min (Case 3.f1), 0.500 mL/min (Case 3), 1 mL/min (Case 3.f2), 5 mL/min (Case 3.f3), and 7.50 mL/min (Case 3.f4). $MgCl_2$ and NaOH concentrations = 0.500 and 1.00 M; stirring speed = 400 rpm; T = 25 °C. The bottom row indicates the employed particle size analyzer: Sympatec HELOS (SH) or Zetasizer Nano (ZN). The upper row reports SEM images.

respectively). In addition, Table 2 reports a case for the double-feed configuration, where no dilution was assumed. The calculated supersaturation level (2.4×10^9) is the highest among the analyzed cases; however, it is most likely over-estimated. As a matter of fact, the two reagent drops cannot react immediately since they dilute in the water bath as they are fed at two opposite reactor sides.

It must be stressed that supersaturation values reported in Table 2 were only estimated based on possible scenarios that could occur in the two investigated feeding mode systems. A more detailed description of the phenomena characterizing the analyzed systems can be provided by coupling computation fluid dynamic (CFD) simulations and population balance equations. Modeling tools can provide a deep interpretation of the influence of mixing conditions, reactant addition rates, reaction time, and reaction evolution on particle sizes, particle morphology, and level of agglomeration/aggregation during the experimental tests.

3.2. $Mg(OH)_2$ Particles Characteristics. The influence of the feeding operating conditions on $Mg(OH)_2$ particles characteristics (median diameters, $d(0.5)$, and morphologies) is introduced in the following sections. Enlarged SEM images are also available in Appendix A.

3.2.1. Single-Feed Configurations. Figure 3 shows the median diameter values obtained for Configurations 1 and 2 at reactant flow rates (Q) of 0.500 and 1.00 mL/min, see Table 1. For Configuration 1, SEM pictures were also reported. The employed $MgCl_2$ and NaOH concentrations were (i) 0.036 and 0.500 M for Configuration 1 and (ii) 0.250 and 0.072 M for Configuration 2.

The reactant flow rate was 0.500 mL/min (Cases 1.f1 and 2.f1) and 1.00 mL/min (Cases 1 and 2). In Figure 3, solid and diagonal stripes bars refer to d(0.5) values calculated before and after PAA-ultrasound treatment (PAA-US), respectively.

At a feeding rate of 1 mL/min (solid red, Case 1, and blue, Case 2, bars), particles are more agglomerated in Case 2, as indicated by the $d(0.5)$ shift before (solid bars) and after (diagonal stripes bars) PAA-US. Before sonication, $d(0.5)$ is equal to ~1.3 μm in Case 2, while it is ~0.12 μm in Case 1. After sonication (diagonal stripes bars), the median diameters decrease down to ~0.10 μm in both Cases. This suggests that the two different configurations produce similar $Mg(OH)_2$ aggregates.

At a feeding rate of 0.500 mL/min, similar agglomerate sizes of ~5.53 and 4.43 μm are observed for Case 1.f1 (solid green bar) and Case 2.f1 (solid orange bar), respectively. After sonication, aggregates are bigger in Case 2.f1 (~0.66 μm, diagonal stripes orange bar) with respect to Case 1.f1 (~0.16 μm, diagonal stripes green bar). Aggregates are always bigger than those produced at lower feeding time (higher flow rate). The bigger agglomerates observed in Case 2 with respect to Case 1 could be ascribed to the higher-pH environment attained during the reaction. At the beginning of the tests, the initial measured pH values were ~10 and ~13 for Case 1 and Case 2, respectively, due to the presence of $MgCl_2$ or NaOH solutions in the reactor. In both cases, the final measured pH value was ~10.5, close to the equilibrium one, indicating the complete conversion of the reagents. pH trends are reported in Appendix A. Particle stability in suspensions can be studied by ζ-potential analyses at different pH values. In the literature, $Mg(OH)_2$ ζ-potential values have been reported to vary from +20 mV at pH 10 to −28 mV at pH 13.5, being null (isoelectric point) at pH ~12.[35,36] Therefore, the ζ-potential values are lower in Case 2 (pH from 13 to 10.5 passing through the isoelectric point) rather than in Case 1 (pH from 10 to 10.5), inducing a higher particle agglomeration. The pH influence is probably overcome by the higher residence time in Cases 1.f1 and 2.f1. The higher residence time may induce a higher particle collision probability leading to bigger agglomerates and aggregates.

For the sake of brevity, only SEM images of Case 1 and Case 1.f1 are reported in the upper row of Figure 3, since similar results were obtained in Cases 2 and 2.f1.

Nanometric globular/flakes primary particles can be observed in both cases. Unfortunately, it is quite difficult to distinguish if particles are more or less aggregated. The presence of globular/flakes particles was somehow expected. As discussed in Section 1, nanometric globular $Mg(OH)_2$ particles are always produced by precipitation with NaOH solutions.[21−23] This can be due to the high supersaturation levels reached during the tests, previously estimated for single-feed configurations. Conse-

https://doi.org/10.1021/acs.cgd.3c00462
Cryst. Growth Des. XXXX, XXX, XXX−XXX

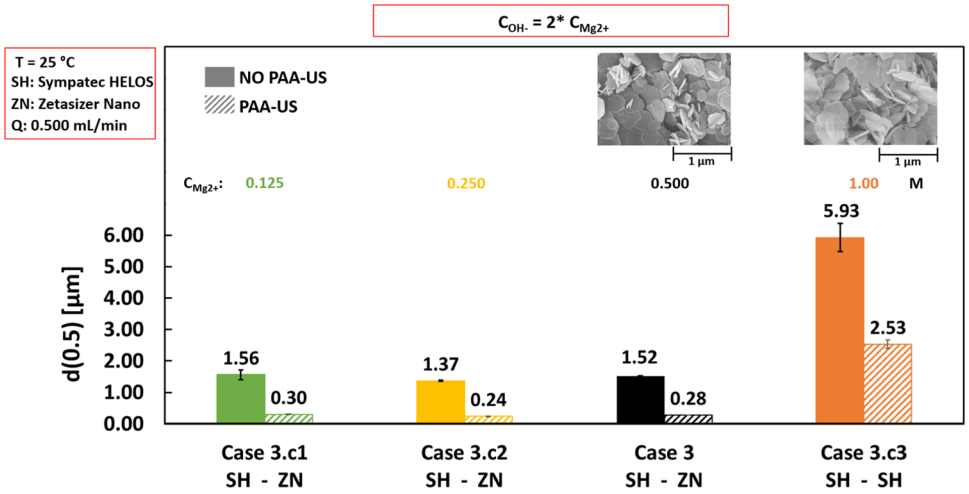


Figure 5. Effect of reactant concentrations on median diameter $d(0.5)$ values calculated before (solid bars) and after (diagonal stripes bars) PAA-US. 0.125, 0.250, 0.500, and 1 M $MgCl_2$ and their NaOH stoichiometric concentrations were employed for Cases 3.c1, 3.c2, 3, and 3.c3, respectively. Flow rates = 0.500 mL/min, stirring speed = 400 rpm, T = 25 °C. The bottom row indicates the employed particle size analyzer: Sympatec HELOS (SH) or Zetasizer Nano (ZN). The upper row reports SEM images.

quently, nucleation and particle aggregation are the predominant phenomena over crystal growth.

3.2.2. Double-Feed Configuration. The influence of (i) reagent flow rates, (ii) reagent concentrations, and (iii) reaction temperature was studied in the double-feed mode, as listed in Table 1.

Solid and diagonal stripes bars refer to $d(0.5)$ values calculated before and after PAA-ultrasound treatment (PAA-US), respectively.

3.2.2.1. Influence of Reactant Flow Rate in Double-Feed Configuration. Figure 4 reports median diameters for Cases 3.f1, 3, 3.f2, 3.f3, and 3.f4 obtained at feed flow rates of 0.250, 0.500, 1, 5.00, and 7.50 mL/min, respectively. In all tests, 0.500 M $MgCl_2$ and 1.00 M NaOH solutions were used.

The upper row of Figure 4 shows SEM pictures for all cases.

Before PAA-US (solid bars), Cases 3.f2 (yellow), 3.f3 (orange), and 3.f4 (blue) are characterized by quite similar median diameters ranging between 0.21 and 0.32 μm. Conversely, bigger agglomerates, above 1 μm, are observed for Case 3 (solid black bar) and even bigger for Case 3.f1 (solid green bar). The same trend is also noticed after PAA-US (diagonal stripes bars), where bigger aggregates are observed for Cases 3.f1 (green) and 3 (black), clearly highlighting the influence of the feeding time on $Mg(OH)_2$ particles. In particular, the higher the feeding time (moving from 6.5 min, Case 3.f4, to 200 min, Case 3.f1), the bigger are the particles. This behavior can be caused by stronger bridge formation between particles promoted by their higher residence time in the reactor. This behavior is in accordance with the results of Configurations 1 and 2. In all cases, particles are found to be characterized by a hexagonal platelets morphology, see the upper row in Figure 4. $Mg(OH)_2$ platelets are better defined moving from the lowest to the highest reagent flow rates, i.e., from left to right in Figure 4.

This result can be ascribed to: (i) the higher reaction time that can promote crystal growth and (ii) the lower supersaturation level attained in the reactor favored by the slower addition of the reactants that can have more time to dilute before reacting. This is in accordance with the pH profile recorded for Case 3, see Appendix A.

In the literature, $Mg(OH)_2$ hexagonal platelets have been reported only (i) using aqueous ammonia solution, (ii) adding additives, or (iii) after hydrothermal treatment due to the dissolution of small crystals allowing the growth of larger ones in the metastable zone (Ostwald ripening). The findings of Figure 4 indicate that the double-feed configuration allows accurate control of the supersaturation level in the precipitation process. The two reactants streams, fed into the water bath from two opposite sides, most likely dilute before they meet and react, thus guaranteeing low supersaturation levels. This is in accordance with the estimation of supersaturation levels presented in Section 3.1. As already mentioned in Section 1, the double-feed configuration can be of considerable interest for the controlled precipitation process of sparingly soluble compounds, such as halides, oxalates, and sulfates.[26,37,38]

3.2.2.2. Influence of Reactant Concentrations in Double-Feed Configuration. Figure 5 shows the median diameters for double-feed Cases 3.c1, Case 3.c2, Case 3, and Case 3.c3 performed adopting $MgCl_2$ concentrations of 0.125, 0.250, 0.500, and 1.00 M, respectively. Stoichiometric NaOH solution concentrations were always employed. The same feed flow rate of 0.500 mL/min and feeding time of 100 min were set in the experiments. For Cases 3 and 3.c3, SEM pictures are shown in the upper row of Figure 5.

Notably, the median diameters of Case 3.c3 (1.00 M $MgCl_2$ and 2.00 M NaOH) show the biggest agglomerates and aggregates (solid and diagonal stripes orange bars in Figure 5) among the other cases. Cases 3.c1, 3.c2, and 3 exhibit quite similar median diameters: agglomerates of ~1.37 to 1.52 μm (solid bars) and aggregates of ~0.24 to 0.30 μm (diagonal stripes bars).

This can be explained by the Derjaguin–Landau–Verwey–Overbeek (DLVO) theory: particles have a higher tendency to agglomerate and aggregate in high-ionic-strength NaCl solutions (here the reaction byproduct) due to the compression of their electrical double layer.[39]

Interestingly, well-defined hexagonal platelets with a primary particle size of around ~300 nm can be clearly observed in Case 3 and even in Case 3.c3, see Figure 5. The double-feed configuration guarantees very low supersaturation values also adopting the highest reactant concentrations (Case 3.c3).

https://doi.org/10.1021/acs.cgd.3c00462
Cryst. Growth Des. XXXX, XXX, XXX−XXX

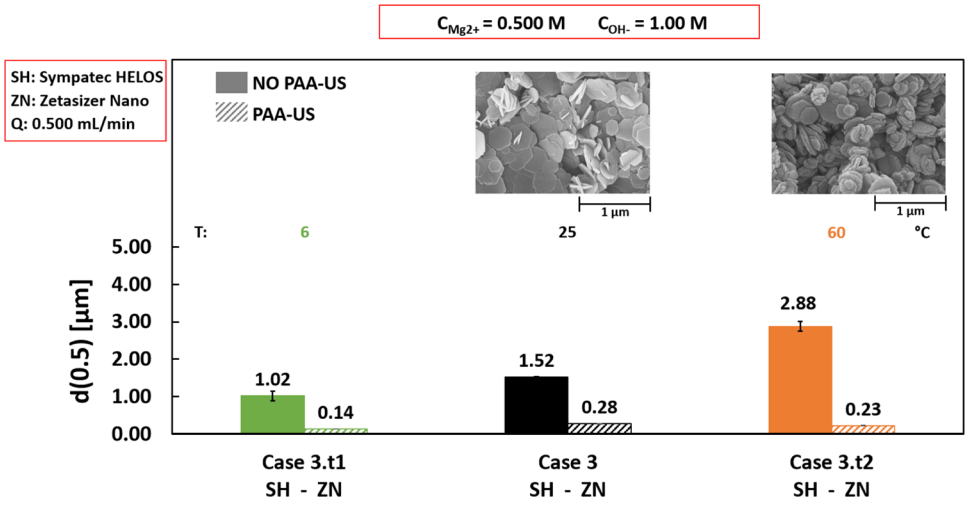


Figure 6. Effect of reaction temperature on median diameter $d(0.5)$ values calculated before (solid bars) and after (diagonal stripes bars) PAA-US. 6, 25 and 60 °C were the reaction temperatures set for Cases 3.t1, 3, and 3.t2, respectively. $MgCl_2$ and NaOH concentrations = 0.500 and 1 M, flow rates = 0.500 mL/min, stirring speed = 400 rpm. The bottom row indicates the employed particle size analyzer: Sympatec HELOS (SH) or Zetasizer Nano (ZN). The upper row reports SEM images.

Table 3. BET Analyses on $Mg(OH)_2$ Powders Obtained in Different Production Routes

authors	production route	BET value	morphology
this work	$MgCl_2$ + NaOH at 25 °C in a double-feed stirred tank reactor (Case 3 and Case 3.f1)	~37 to 45 m^2/g	hexagonal platelets
Henrist et al.[11]	$MgCl_2$ + NH_4OH at 25 °C in a controlled double-jet stirred tank reactor	~21 m^2/g	hexagonal platelets
Henrist et al.[11]	$MgCl_2$ + NH_4OH at 25 °C in controlled double-jet stirred tank reactor 1-week hydrothermal treatment at 170 °C	~2 m^2/g	hexagonal platelets
Wu et al.[25]	$MgCl_2$ + NaOH at 25 °C in a single-feed stirred tank reactor after the addition of 1 g/L of $CaCl_2$ and 4 h hydrothermal treatment at 160 °C	~29 m^2/g	hexagonal platelets
Ren et al.[7]	$MgCl_2$ + NaOH at 70 °C in T-mixer	~90 m^2/g	nanoflakes/globular
Mullin et al.[24]	$MgCl_2$ + NaOH at 25 °C in single-feed stirred tank reactor	~110 to 140 m^2/g	nanoflakes/globular

Therefore, no SEM images were collected for Cases 3.c1 and 3.c2, as they are expected to be similar to Case 3.

3.2.2.3. Influence of Temperature on Double-Feed Configuration. Figure 6 reports the median diameters for Cases 3.t1, 3, and 3.t2 conducted at reaction temperatures of 6, 25, and 60 °C, respectively. In all tests, 0.500 M $MgCl_2$ and 1.0 M NaOH solutions were used and pumped at 0.500 mL/min.

Before PAA-US (solid bars), agglomerates median diameters increase slightly with the increased reaction temperature. While a not clear trend is noticed after PAA-US (diagonal stripes bars), similar aggregates of ~0.14, ~0.28, and ~0.23 μm are measured for Cases 3.t1 (6 °C), 3 (25 °C), and 3.t2 (60 °C), respectively. Overall, the temperature does not considerably influence the precipitation process, as also confirmed by SEM images. Similar morphology, in fact, is detected for Cases 3 (25 °C) and 3.t2 (60 °C), see Figure 6.

3.3. BET Comparison between Particles. A fundamental parameter to identify the industrial suitability of $Mg(OH)_2$ powders is the particle's specific surface area. To assess this parameter, selected samples were analyzed by the BET technique as discussed in Section 2.2. Table 3 reports the obtained values for grown hexagonal $Mg(OH)_2$ platelets, from Cases 3.f1 and 3, in double-feed configuration. A comparison of specific surface areas reported in the literature is also presented.

Samples produced in Cases 3 and 3.f1 are characterized by specific surface area values ranging from ~37 to 45 m^2/g. These values are still 4 times higher than those required for flame-retardant applications (~10 m^2/g); however, they are among the lowest ever reported when NaOH is employed to precipitate $Mg(OH)_2$ compounds. Considerably higher surface area values were reported by Ren et al.[7] (~90 m^2/g), using a T-mixer, and Mullin et al.[24] (~110 to 140 m^2/g), employing a stirred tank in single-feed mode. These values can be due to high super-saturation levels, high nucleation rate, and thus, a huge number of nanosized particles. As discussed in Section 1, specific surface area values lower than those of Cases 3.f1 and 3 were obtained only after hydrothermal treatment or using NH_4OH.[11,25]

4. CONCLUSIONS

The magnesium hydroxide precipitation process, from synthetic $MgCl_2$ and NaOH solutions, was experimentally explored in unseeded stirred tank crystallizers in single- and double-feed configurations. The challenge was to identify the best operating conditions to favor crystal growth in a process dominated by nucleation. The influence of reactant flow rates (feeding times), $MgCl_2$ and NaOH concentrations, and reaction temperature was analyzed.

In single-feed modes, at the highest flow rates (1 mL/min), the addition of $MgCl_2$ solutions into a NaOH bath led to bigger agglomerates than those observed when adding NaOH solutions into the $MgCl_2$ bath. This behavior was attributed to the higher reaction pH environment attained in the NaOH bath that promoted particle agglomeration. At the lowest flow rates (0.5 mL/min) (the highest feeding time), larger and stronger agglomerates and aggregates were identified. For these cases, the pH influence was probably overcome by the greater feeding

https://doi.org/10.1021/acs.cgd.3c00462
Cryst. Growth Des. XXXX, XXX, XXX−XXX

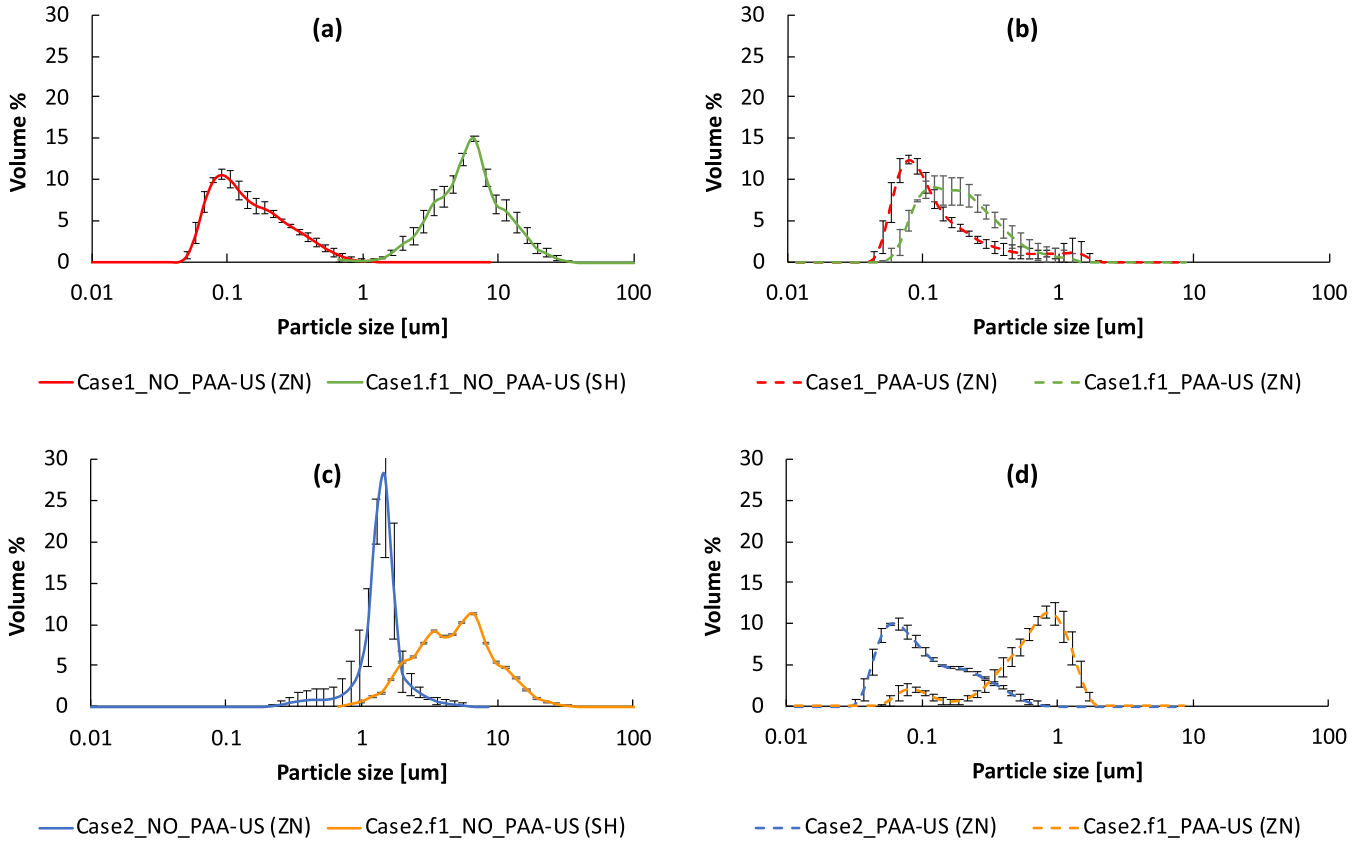


Figure 7. PSDs collected for single-feed cases. Configuration 1 using 0.036 M $MgCl_2$ and 0.500 M NaOH (a) before and (b) after PAA-US; Configuration 2 at 0.250 M $MgCl_2$ and 0.072 M NaOH (c) before and (d) after PAA-US. In brackets, the employed particle size analyzer: Sympatec HELOS (SH) or Zetasizer Nano (ZN). Feed flow rate = 1.00 mL/min (Cases 1 and 2) and 0.500 mL/min (Cases 1.f1 and 2.f1), stirring speed = 400 rpm, T = 25 °C.

Table A1. $d(0.1)$, $d(0.5)$, and $d(0.9)$ Calculated from PSDs Collected before PAA-US for Cases 1, 1.f1, 2, and 2.f1 in Single-Feed Configuration

	case 1		case 1.f1		case 2		case 2.f1	
	average	STD dev	average	STD dev	average	STD dev	average	STD dev
$d0.1$ [μm]	0.066	0.003	2.620	0.219	0.864	0.266	1.822	0.007
$d0.5$ [μm]	0.120	0.001	5.533	0.540	1.301	0.092	4.428	0.028
$d0.9$ [μm]	0.333	0.036	12.054	1.282	1.792	0.079	10.640	0.171

time, which caused a stronger aggregation between primary particles due to the higher particle collision probability in the reactor. The same behavior was observed in double-feed configuration: at decreasing flow rates, increasingly strong agglomerates and aggregates were detected.

In double-feed configuration, (i) at the highest solutions concentration, stronger agglomerates and aggregates were precipitated, probably due to the increase of the solution ionic strength and (ii) no impact of the reaction temperature on agglomerate and aggregate size was observed.

Nanoflakes primary particles with a primary particle size of 50−70 nm were detected in all single-feed experiments, regardless of the reactant feeding configuration or reactant concentrations.

Conversely, well-defined $Mg(OH)_2$ hexagonal platelets (especially at low feed flow rates) with a primary particle size of 300−350 nm and characterized by specific surface area values of ∼40 m^2/g were successfully synthesized in double-feed tests using NaOH solutions. This was achieved thanks to the very accurate control of supersaturation in the system. Specific surface areas reported in the double-feed configurations are still 4 times higher than those required for flame retard applications. Nevertheless, the present work paves the road for a promising precipitation route to produce $Mg(OH)_2$ hexagonal platelets using NaOH solutions.

APPENDIX A

In this appendix, for the sake of completeness, average volume PSDs and characteristic diameters, e.g., $d(0.1)$, $d(0.5)$, and $d(0.9)$, for all discussed cases (Table 1) are reported. In addition, pH profiles measured for Cases 1, 2, and 3 are shown. A preliminary estimation of the influence of mixing time, reactants addition rates, and reaction time on particle size is also provided.

The solid and dashed lines indicate PSDs obtained before and after PAA and ultrasound treatment (PAA-US), respectively. The employed particle size analyzer is reported in parentheses: Sympatec HELOS (SH) or Zetasizer Nano (ZN).

https://doi.org/10.1021/acs.cgd.3c00462
Cryst. Growth Des. XXXX, XXX, XXX−XXX

Table A2. $d(0.1)$, $d(0.5)$, and $d(0.9)$ Calculated from PSDs Collected after PAA-US for Cases 1, 1.f1, 2, and 2.f1 in Single-Feed Configuration

	case 1 PAA-US		case 1.f1 PAA-US		case 2 PAA-US		case 2.f1 PAA-US	
	average	STD dev	average	STD dev	average	STD dev	average	STD dev
$d0.1$ [μm]	0.058	0.005	0.082	0.007	0.045	0.002	0.159	0.059
$d0.5$ [μm]	0.097	0.007	0.163	0.008	0.084	0.004	0.660	0.068
$d0.9$ [μm]	0.554	0.333	0.436	0.127	0.268	0.023	1.154	0.078

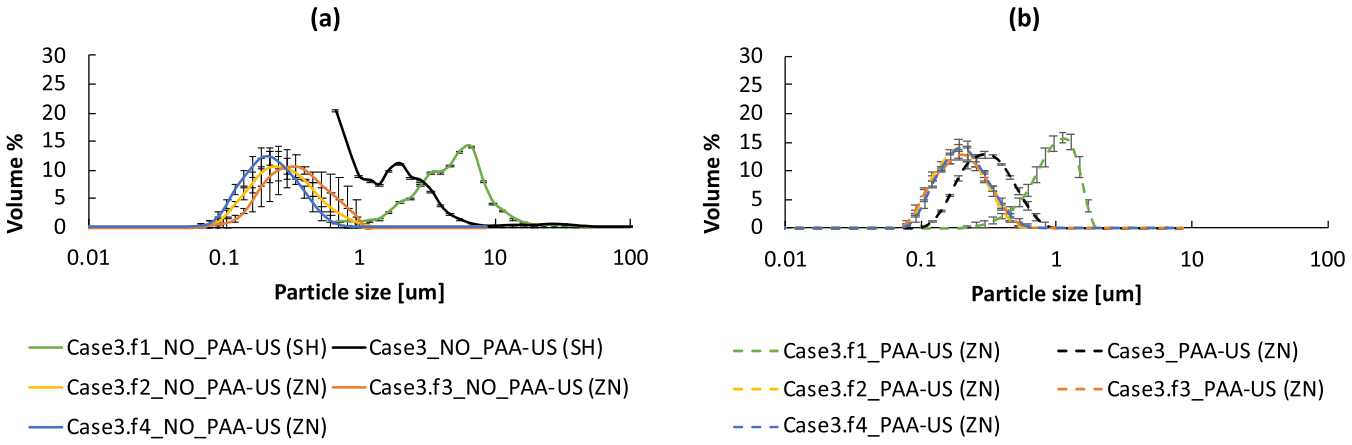


Figure 8. Effect of feeds flow rate on $Mg(OH)_2$ particles before (a) and after (b) PAA-US. In brackets, the employed particle size analyzer: Sympatec HELOS (SH) or Zetasizer Nano (ZN). Flow rates of 0.250 mL/min (Case 3.f1), 0.500 mL/min (Case 3), 1.00 mL/min (Case 3.f2), 5 mL/min (Case 3.f3), and 7.50 mL/min (Case 3.f4). $MgCl_2$ and NaOH concentrations = 0.500 and 1.00 M, stirring speed = 400 rpm, T = 25 °C.

Table A3. $d(0.1)$, $d(0.5)$, and $d(0.9)$ Calculated from PSDs Collected before PAA-US for Cases 3.f1, 3, 3.f2, 3.f3, and 3.f4 in Double-Feed Configuration[a]

	case 3.f1		case 3		case 3.f2		case 3.f3		case 3.f4	
	average	STD dev	average	STD dev	average	STD dev	average	STD dev	average	STD dev
$d0.1$ [μm]	1.868	0.007			0.131	0.005	0.157	0.008	0.114	0.007
$d0.5$ [μm]	4.397	0.016	1.522	0.007	0.255	0.034	0.318	0.065	0.205	0.014
$d0.9$ [μm]	8.521	0.143	3.496	0.073	0.504	0.129	0.600	0.160	0.375	0.046

[a]Some $d(0.1)$ data are missing because the granulometric analysis resulted in a PSD where the first discrete range of revealed size (bin: 0.5−0.9 μm) is already more than 10% in volume, higher than the $d(0.1)$.

Table A4. $d(0.1)$, $d(0.5)$, and $d(0.9)$ Calculated from PSDs Collected after PAA-US for Cases 3.f1, 3, 3.f2, 3.f3 and 3.f4 in Double-Feed Configuration

	case 3.f1 PAA-US		case 3 PAA-US		case 3.f2 PAA-US		case 3.f3 PAA-US		case 3.f4 PAA-US	
	average	STD dev	average	STD dev	average	STD dev	average	STD dev	average	STD dev
$d0.1$ [μm]	0.498	0.037	0.163	0.001	0.108	0.004	0.106	0.006	0.114	0.007
$d0.5$ [μm]	0.914	0.039	0.280	0.007	0.179	0.005	0.184	0.006	0.189	0.001
$d0.9$ [μm]	1.357	0.047	0.488	0.025	0.301	0.001	0.324	0.006	0.329	0.030

A.1. PSDs and Characteristic Diameters Collected for Single-Feed Cases (Section 3.2.1)

Figure 7 reports PSD measurements of Cases 1, 1.f1, 2, and 2.f1 in single-feed configuration, before (a, c) and after (b, d) PAA-US treatment.

Tables A1 and AA2 report $d(0.1)$, $d(0.5)$, and $d(0.9)$ calculated from PSDs measurements of Cases 1, 1.f1, 2, and 2.f1 in single-feed configuration, before (Table A1) and after (Table A2) PAA-US.

A.2. PSDs and Characteristic Diameters Collected for Double-Feed Cases (Section 3.2.2)

A.2.1. Influence of Reactant Flow Rate (Section 3.2.2.1). Figure 8 reports PSD measurements of Cases 3.f1, 3, 3.f2, 3.f3, and 3.f4 in double-feed configuration, before (a) and after (b) PAA-US treatment.

Tables A3 and AA4 report $d(0.1)$, $d(0.5)$ and $d(0.9)$ calculated from PSD measurements of Cases 3.f1, 3, 3.f2, 3.f3, and 3.f4 in double-feed configuration, before (Table A3) and after (Table A4) PAA-US.

A.2.2. Influence of Reactant Concentrations (Section 3.2.2.2). Figure 9 reports PSD measurements of Cases 3.c1, 3.c2, 3, and 3.c3 in double-feed configuration, before (a) and after (b) PAA-US treatment.

Tables A5 and AA6 report $d(0.1)$, $d(0.5)$, and $d(0.9)$ calculated from PSD measurements of Cases 3.c1, 3.c2, 3, and 3.c3 in double-feed configuration, before (Table A5) and after (Table A6) PAA-US.

https://doi.org/10.1021/acs.cgd.3c00462
Cryst. Growth Des. XXXX, XXX, XXX−XXX

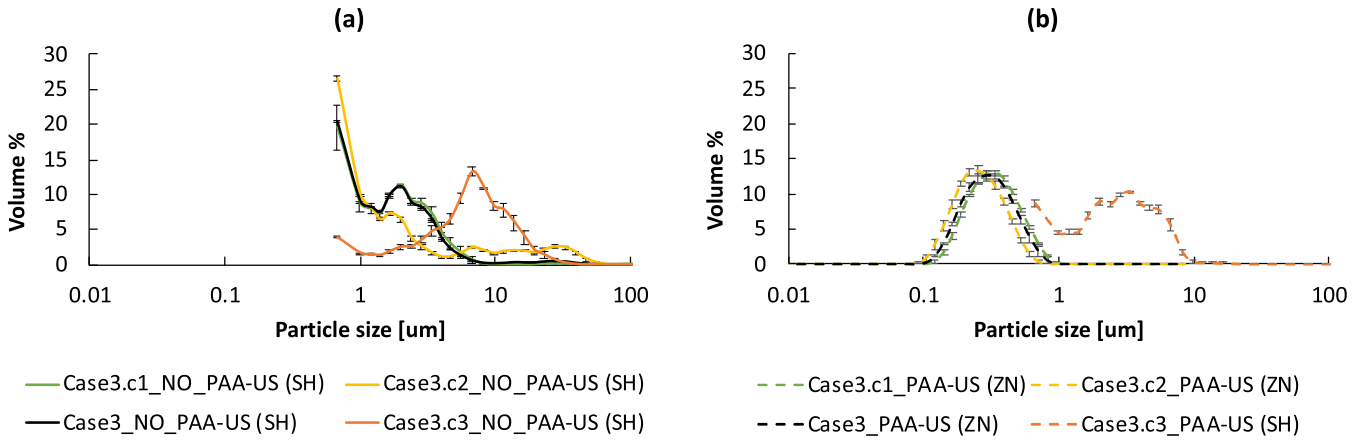


Figure 9. Effect of reactants' concentrations on $Mg(OH)_2$ particles before (a) and after (b) PAA-US. In parentheses, the employed device: Sympatec HELOS (SH) and Zetasizer Nano (ZN). 0.125, 0.250, 0.500, and 1.00 M $MgCl_2$ and their NaOH stoichiometric concentration were employed for Cases 3.c1, 3.c2, 3, and 3.c3, respectively. Flow rates = 0.500 mL/min, stirring speed = 400 rpm, T = 25 °C.

Table A5. $d(0.1)$, $d(0.5)$, and $d(0.9)$ Calculated from PSDs Collected before PAA-US for Cases 3.c1, 3.c2, 3, and 3.c3 in Double-Feed Configuration[a]

	case 3.c1		case 3.c2		case 3		case 3.c3	
	average	STD dev	average	STD dev	average	STD dev	average	STD dev
$d0.1$ [μm]							1.606	0.080
$d0.5$ [μm]	1.563	0.152	1.372	0.019	1.522	0.007	5.926	0.445
$d0.9$ [μm]	3.439	0.360	3.474	0.125	3.496	0.073	13.019	1.141

[a]Some $d(0.1)$ data are missing because the granulometric analysis resulted in a PSD where the first discrete range of revealed size (bin: 0.5−0.9 μm) is already more than 10% in volume, higher than the $d(0.1)$.

Table A6. $d(0.1)$, $d(0.5)$, and $d(0.9)$ Calculated from PSDs Collected before PAA-US for Cases 3.c1, 3.c2, 3, and 3.c3 in Double-Feed Configuration

	case 3.c1 PAA-US		case 3.c2 PAA-US		case 3 PAA-US		case 3.c3 PAA-US	
	average	STD dev	average	STD dev	average	STD dev	average	STD dev
$d0.1$ [μm]	0.178	0.005	0.143	0.006	0.163	0.001	0.763	0.044
$d0.5$ [μm]	0.304	0.006	0.239	0.006	0.280	0.007	2.532	0.130
$d0.9$ [μm]	0.525	0.005	0.409	0.013	0.488	0.025	5.302	0.271

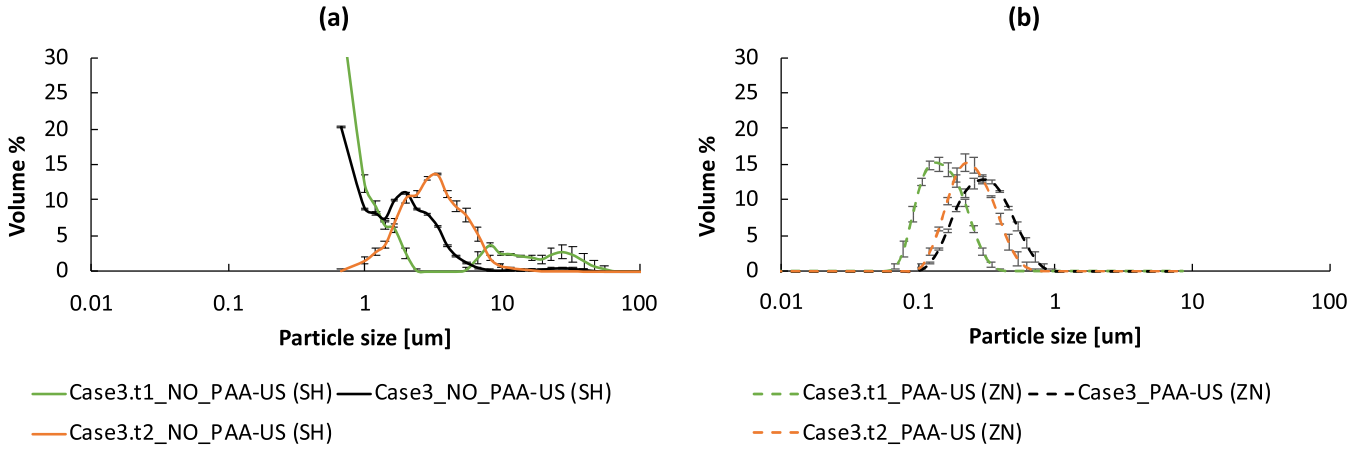


Figure 10. Effect of reaction temperature on $Mg(OH)_2$ final particles before (a) and after (b) PAA-US. In parentheses, the employed device: Sympatec HELOS (SH) and Zetasizer Nano (ZN). 6 °C, 25 °C, and 60 °C were the reaction temperatures set for Cases 3.t1, 3, and 3.t2, respectively. $MgCl_2$ and NaOH concentrations = 0.500 and 1.00 M, Flow rates = 0.500 mL/min, stirring speed = 400 rpm.

A.2.3. Influence of Reactant Concentrations (Section 3.2.2.3). Figure 10 reports PSD measurements of Cases 3.t1, 3, and 3.t2 in double-feed configuration, before (a) and after (b) PAA-US treatment.

Tables A7 and AA8 report $d(0.1)$, $d(0.5)$, and $d(0.9)$ calculated from PSDs measurements of Cases 3.t1, 3, and 3.t2 in double-feed configuration, before (Table A7) and after (Table A8) PAA-US.

https://doi.org/10.1021/acs.cgd.3c00462
Cryst. Growth Des. XXXX, XXX, XXX−XXX

Table A7. $d(0.1)$, $d(0.5)$, and $d(0.9)$ Calculated from PSDs Collected before PAA-US for Cases 3.t1, 3, and 3.t2 in Double-Feed Configuration[a]

	case 3.t1		case 3		case 3.t2	
	average	STD dev	average	STD dev	average	STD dev
$d0.1$ [μm]					1.468	0.063
$d0.5$ [μm]	1.018	0.134	1.522	0.007	2.876	0.130
$d0.9$ [μm]	4.902	0.099	3.496	0.073	5.390	0.160

[a]Some $d(0.1)$ data are missing because the granulometric analysis resulted in a PSD where the first discrete range of revealed size (bin: 0.5−0.9 μm) is already more than 10% in volume, thus preventing from having the $d(0.1)$.

Table A8. $d(0.1)$, $d(0.5)$, and $d(0.9)$ Calculated from PSDs Collected before PAA-US for Cases 3.t1, 3, and 3.t2 in Double-Feed Configuration

	case 3.t1 PAA-US		case 3 PAA-US		case 3.t2 PAA-US	
	average	STD dev	average	STD dev	average	STD dev
$d0.1$ [μm]	0.089	0.004	0.163	0.001	0.143	0.003
$d0.5$ [μm]	0.137	0.004	0.280	0.007	0.225	0.007
$d0.9$ [μm]	0.221	0.006	0.488	0.025	0.369	0.029

A.3. pH Profiles of Cases 1, 2, and 3

pH profiles were collected in Cases 1, 2, and 3. Figure 11 shows the pH profiles of Cases 1 and 2 in single-feed configuration.

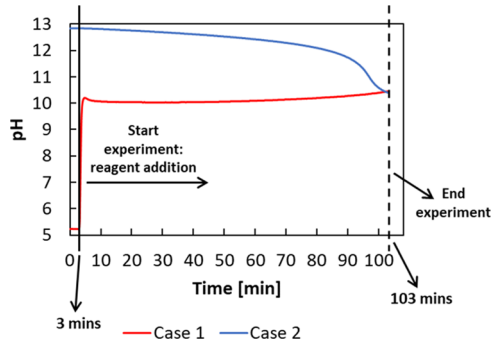


Figure 11. pH profiles along time for Cases 1 (red solid line) and 2 (blue solid line). NaOH solution (Case 1) and $MgCl_2$ solution (Case 2) addition began at 3 min and lasted 100 min (final experimental time of 103 min).

As can be observed, at the beginning of the feed addition, the initial measured pH values were about 10 and 13 for Case 1 (red solid line) and Case 2 (blue solid line), respectively, due to the initial solution contained within the reactor, i.e., $MgCl_2$ for Case 1 and NaOH for Case 2.

pH slowly increased from 10 to 10.5 in Case 1, while it slowly decreased from 13 to 12 and then rapidly, at the end of the test, to 10.5 in Case 2. In both cases, the final measured pH value of 10.5, close to the equilibrium one, indicated the complete conversion of the reagents.

In addition, the pH profile of Case 3 in double-feed configuration is shown in Figure 12.

As can be seen, pH profiles rapidly increased from 5 to 10 after reagent addition, slowly reaching 11, before decreasing to the equilibrium pH value of 10.5. It is worth noting that a similar pH profile was found in Case 1, see Figure 11, but, as widely discussed in Section 3.1, the reagents drop dilution, before the reaction, changes depending on the feeding configurations.

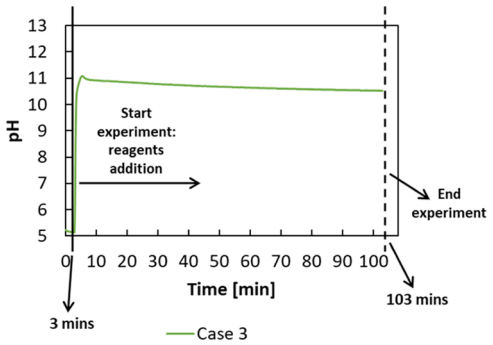


Figure 12. pH profiles along time for Case 3 (green solid line). The addition of $MgCl_2$ and NaOH solutions began at 3 min and lasted 100 min (final experimental time of 103 min).

Therefore, the local pH measurement in a double-feed configuration is closer to the reaction environment due to higher reagents homogenization before reacting.

A.4. Preliminary Estimation of the Influence of Mixing Time, Reactants Addition Rates, and Reaction Time on Particles Size

A preliminary analysis on the influence of mixing, reagents addition, and reaction times on particle sizes was carried out considering the results obtained for Cases 3.f1, 3, 3.f2, 3.f3, and 3.f4 (reagents flow rates of 0.250, 0.500, 1.00, 5.00 and 7.50 mL/min, respectively). The concentrations of $MgCl_2$ and NaOH solutions were always 0.500 and 1.00 M.

In precipitation processes, the Damköhler number is the timescale ratio between the mixing and solid formation (reaction time)

$$Da = \frac{t_m}{t_r} \tag{2}$$

where t_m is the mixing time and t_r is the chemical reaction time. Both mixing and reaction times can be better addressed by process modeling of a system. In the present work, a preliminary estimation is conducted. The reaction time was assumed to be equal to the induction one (t_{ind}), which is the time that elapses between the onset of supersaturation and the formation of a solid phase. This assumption is likely an underestimation, as the experimental induction time is typically longer than the reaction one (solids must reach a detectable size to be observed[40]). However, the induction time was adopted since experimental data with respect to supersaturation levels are available in the literature.[18,41] The mixing time, as discussed in Section 2.1, was estimated to be equal to 15 s.

Nevertheless, the supersaturation value inside the tank was determined by assuming a perfect mixing condition at each instant of experimental tests; consequently, the induction time is evaluated for each supersaturation value.

Figure 13 shows the induction time (t_{ind}) trends as a function of the time estimated for Cases 3.f1, 3, 3.f2, 3.f3, and 3.f4.

In Figure 13, two regions are delineated by a red horizontal dashed line ($Da \approx 1$). Above the dashed line, the induction time is higher than the mixing time ($Da < 1$) and thus the precipitation rate is the rate-determining step; conversely, below, the precipitation rate becomes faster than the mixing ($Da > 1$). In this latter region, mixing is the rate-determining step that is not enough adequate to ensure a good reactants homogenization before the reaction (possible local supersaturation hotspot).

https://doi.org/10.1021/acs.cgd.3c00462
Cryst. Growth Des. XXXX, XXX, XXX−XXX

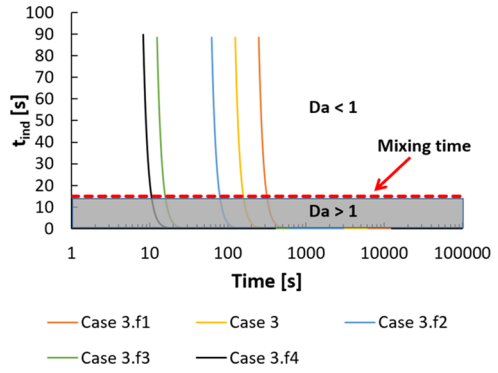


Figure 13. Induction time (t_{ind}) versus time for Cases 3.f1 (0.250 mL/min), 3 (0.500 mL/min), 3.f2 (1.00 mL/min), 3.f3 (5.00 mL/min), and 3.f4 (7.5 mL/min). $MgCl_2$ and NaOH concentrations: 0.500 and 1.00 M; stirring rate = 400 rpm; temperature = 25 °C. A relation between supersaturation and induction time was obtained from experimental data looking at Table 1 of Yuan et al.[18]

At increasing flow rates, the time at which $Da \approx 1$ decreases due to the faster reactants addition rate and thus the higher supersaturation level, as can be clearly observed in Figure 14.

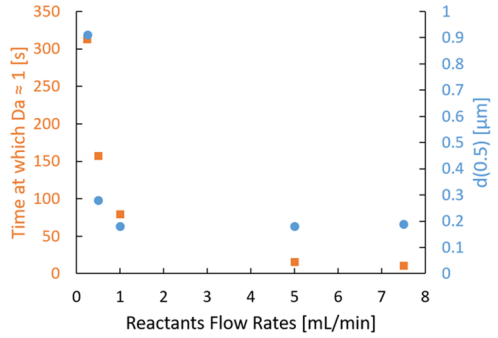


Figure 14. Characteristic diameter, $d(0.5)$, values after PAA-US and time at which $Da \approx 1$ as a function of reactant flow rates for Cases 3.f1 (0.250 mL/min), 3 (0.500 mL/min), 3.f2 (1.00 mL/min), 3.f3 (5.00 mL/min), and 3.f4 (7.5 mL/min). $MgCl_2$ and NaOH concentrations: 0.500 and 1.00 M; stirring rate = 400 rpm; temperature = 25 °C. $d(0.5)$ shows a plateau already at a reactant flow rate of 1 mL/min. This indicates that the high supersaturation levels achieved in short times promote nucleation phenomena rather than crystal growth, causing a decrease in characteristic diameter $d(0.5)$.

Figure 14 shows also the characteristic diameter, $d(0.5)$, values with PAA-US as a function of reactant flow rates.

■ ASSOCIATED CONTENT

Supporting Information

The Supporting Information is available free of charge at https://pubs.acs.org/doi/10.1021/acs.cgd.3c00462.

Enlarged images of SEM analyses; comparison between particle size distributions for Cases 3 and 3.c1 obtained by adopting the SYMPATEC HELOS and the Zetasizer Nano devices; SEM micrographs at different locations of the same sample for Cases 1.f1, 1, 3, and 3.f4 (SEM statistical relevance); and repeatability and reproducibility analyses (PDF)

■ AUTHOR INFORMATION

Corresponding Author

Giuseppe Battaglia − *Dipartimento di Ingegneria, Università degli studi di Palermo, 90128 Palermo, Italy;* orcid.org/0000-0001-8094-0710; Email: giuseppe.battaglia03@unipa.it

Authors

Salvatore Romano − *Dipartimento di Ingegneria, Università degli studi di Palermo, 90128 Palermo, Italy*

Silvio Trespi − *Institute of Energy and Process Engineering, ETH Zurich, 8092 Zurich, Switzerland*

Ramona Achermann − *Institute of Energy and Process Engineering, ETH Zurich, 8092 Zurich, Switzerland*

Antonello Raponi − *Department of Applied Science and Technology, Institute of Chemical Engineering, Politecnico di Torino, 10129 Torino, Italy;* orcid.org/0000-0002-3951-2308

Daniele Marchisio − *Department of Applied Science and Technology, Institute of Chemical Engineering, Politecnico di Torino, 10129 Torino, Italy*

Marco Mazzotti − *Institute of Energy and Process Engineering, ETH Zurich, 8092 Zurich, Switzerland;* orcid.org/0000-0002-4948-6705

Giorgio Micale − *Dipartimento di Ingegneria, Università degli studi di Palermo, 90128 Palermo, Italy*

Andrea Cipollina − *Dipartimento di Ingegneria, Università degli studi di Palermo, 90128 Palermo, Italy;* orcid.org/0000-0003-0570-195X

Complete contact information is available at: https://pubs.acs.org/10.1021/acs.cgd.3c00462

Author Contributions

S.R.: Conceptualization, methodology, validation, formal analysis, investigation, data curation, visualization, writing—original draft, visualization. S.T.: Conceptualization, methodology, validation, formal analysis, data curation, writing—review and editing, visualization. R.A.: Conceptualization, methodology, validation, writing—review and editing, visualization. G.B.: Conceptualization, methodology, formal analysis, data curation, writing—original draft, visualization, supervision. A.R.: Conceptualization, methodology, validation, visualization. D.M.: Conceptualization, methodology, writing—review and editing, visualization, supervision, project administration, funding acquisition. M.M.: Conceptualization, methodology, resources, writing—review and editing, visualization, supervision, project administration, funding acquisition. G.M.: Conceptualization, methodology, visualization, supervision, project administration, funding acquisition. A.C.: Conceptualization, methodology, writing—review and editing, visualization, supervision, project administration, funding acquisition.

Notes

The authors declare no competing financial interest.

■ ACKNOWLEDGMENTS

This work was partially funded by the European Union's Horizon 2020 Research and Innovation Programme under Grant Agreement No. 869467 (SEArcularMINE). This output reflects only the author's view. The European Health and Digital Executive Agency (HaDEA) and the European Commission cannot be held responsible for any use that may be made of the information contained therein. This research has been partially

https://doi.org/10.1021/acs.cgd.3c00462
Cryst. Growth Des. XXXX, XXX, XXX−XXX

funded by the European Research Council (ERC) under the European Union's Horizon 2020 Research and Innovation Program under Grant Agreement No. 788607. The authors are grateful to Luca Bosetti for the fruitful discussions about the topic and the experimental results, Markus Huber and Sarah Kienast for providing SEM images, and Daniel Trottmann for the technical assistance in the laboratory.

■ ABBREVIATIONS

PAA, poly(acrylic acid, sodium salt); PSD, particle size distribution; US, ultrasound treatment; SLS, static light scattering; DLS, dynamic light scattering; SEM, scanning electron microscopy technique; BET, Brunauer–Emmett–Teller; SH, SYMPATEC HELOS granulometer; ZN, Zetasizer Nano ZS

■ REFERENCES

(1) European Commission. *Study on the EU's List of Critical Raw Materials*, 2020.
(2) Cipollina, A.; Bevacqua, M.; Dolcimascolo, P.; Tamburini, A.; Brucato, A.; Glade, H.; Buether, L.; Micale, G. Reactive Crystallisation Process for Magnesium Recovery from Concentrated Brines. *Desalin. Water Treat.* **2015**, *55*, 2377–2388.
(3) Battaglia, G.; Domina, M. A.; Lo Brutto, R.; Lopez Rodriguez, J.; Fernandez de Labastida, M.; Cortina, J. L.; Pettignano, A.; Cipollina, A.; Tamburini, A.; Micale, G. Evaluation of the Purity of Magnesium Hydroxide Recovered from Saltwork Bitterns. *Water* **2023**, *15*, 29.
(4) Morgante, C.; Vassallo, F.; Battaglia, G.; Cipollina, A.; Vicari, F.; Tamburini, A.; Micale, G. Influence of Operational Strategies for the Recovery of Magnesium Hydroxide from Brines at a Pilot Scale. *Ind. Eng. Chem. Res.* **2022**, *61*, 15355–15368.
(5) Pilarska, A. A.; Klapiszewski, Ł.; Jesionowski, T. Recent Development in the Synthesis, Modification and Application of Mg(OH)2 and MgO: A Review. *Powder Technol.* **2017**, *319*, 373–407.
(6) Montes-Hernandez, G.; Renard, F.; Chiriac, R.; Findling, N.; Toche, F. Rapid Precipitation of Magnesite Microcrystals from $Mg(OH)_2$-H_2O-CO_2 Slurry Enhanced by NaOH and a Heat-Aging Step (from ∼20 to 90 °C). *Cryst. Growth Des.* **2012**, *12*, 5233–5240.
(7) Ren, M.; Yang, M.; Li, S.; Chen, G.; Yuan, Q. High Throughput Preparation of Magnesium Hydroxide Flame Retardant via Micro-reaction Technology. *RSC Adv.* **2016**, *6*, 92670–92681.
(8) Zhuo, L.; Ge, J.; Cao, L.; Tang, B. Solvothermal Synthesis of CoO, Co_3O_4, $Ni(OH)_2$ and $Mg(OH)_2$ Nanotubes. *Cryst. Growth Des.* **2009**, *9*, 1–6.
(9) Xu, B.; Li, T.; Zhang, Y.; Zhang, Z.; Liu, X.; Zhao, J. New Synthetic Route and Characterization of Magnesium Borate Nanorods. *Cryst. Growth Des.* **2008**, *8*, 1218–1222.
(10) Balducci, G.; Bravo Diaz, L.; Gregory, D. H. Recent Progress in the Synthesis of Nanostructured Magnesium Hydroxide. *CrystEngComm* **2017**, *19*, 6067–6084.
(11) Henrist, C.; Mathieu, J.-P.; Vogels, C.; Rulmont, A.; Cloots, R. Morphological Study of Magnesium Hydroxide Nanoparticles Precipitated in Dilute Aqueous Solution. *J. Cryst. Growth* **2003**, *249*, 321–330.
(12) Wang, P.; Li, C.; Gong, H.; Wang, H.; Liu, J. Morphology Control and Growth Mechanism of Magnesium Hydroxide Nanoparticles via a Simple Wet Precipitation Method. *Ceram. Int.* **2011**, *37*, 3365–3370.
(13) Li, X.; Ma, G. B.; Liu, Y. Y. Synthesis and Characterization of Magnesium Hydroxide Using a Bubbling Setup. *Ind. Eng. Chem. Res.* **2009**, *48*, 763–768.
(14) Li, X.; Shi, T.; Chang, P.; Hu, H.; Xie, J.; Liu, Y. Preparation of Magnesium Hydroxide Flame Retardant from Light Calcined Powder by Ammonia Circulation Method. *Powder Technol.* **2014**, *260*, 98–104.
(15) Alamdari, A.; Rahimpour, M. R.; Esfandiari, N.; Nourafkan, E. Kinetics of Magnesium Hydroxide Precipitation from Sea Bittern. *Chem. Eng. Process.: Process Intensif.* **2008**, *47*, 215–221.
(16) Song, X.; Sun, S.; Zhang, D.; Wang, J.; Yu, J. Synthesis and Characterization of Magnesium Hydroxide by Batch Reaction Crystallization. *Front. Chem. Sci. Eng.* **2011**, *5*, 416–421.
(17) Turek, M.; Gnot, W. Precipitation of Magnesium Hydroxide from Brine. *Ind. Eng. Chem. Res.* **1995**, *34*, 244–250.
(18) Yuan, Q.; Lu, Z.; Zhang, P.; Luo, X.; Ren, X.; Golden, T. D. Study of the Synthesis and Crystallization Kinetics of Magnesium Hydroxide. *Mater. Chem. Phys.* **2015**, *162*, 734–742.
(19) Baldyga, J.; Podgórska, W.; Pohorecki, R. Mixing-Precipitation Model with Application to Double Feed Semibatch Precipitation. *Chem. Eng. Sci.* **1995**, *50*, 1281–1300.
(20) Vicum, L.; Mazzotti, M. Multi-Scale Modeling of a Mixing-Precipitation Process in a Semibatch Stirred Tank. *Chem. Eng. Sci.* **2007**, *62*, 3513–3527.
(21) Battaglia, G.; Romano, S.; Raponi, A.; Marchisio, D.; Ciofalo, M.; Tamburini, A.; Cipollina, A.; Micale, G. Analysis of Particles Size Distributions in Mg(OH)2 Precipitation from Highly Concentrated MgCl2 Solutions. *Powder Technol.* **2022**, *398*, No. 117106.
(22) Tai, C. Y.; Tai, C.-T.; Chang, M.-H.; Liu, H.-S. Synthesis of Magnesium Hydroxide and Oxide Nanoparticles Using a Spinning Disk Reactor. *Ind. Eng. Chem. Res.* **2007**, *46*, 5536–5541.
(23) Shen, H.; Liu, Y.; Song, B. Preparation and Characterization of Magnesium Hydroxide Nanoparticles in a Novel Impinging Stream-Rotating Packed Bed Reactor. *J. Chem. Eng. Jpn.* **2016**, *49*, 372–378.
(24) Mullin, J. W.; Murphy, J. D.; Sohnel, O.; Spoors, G. Aging of Precipitated Magnesium Hydroxide. *Ind. Eng. Chem. Res.* **1989**, *28*, 1725–1730.
(25) Wu, Q. L.; Xiang, L.; Jin, Y. Influence of CaCl2 on the Hydrothermal Modification of Mg(OH)2. *Powder Technol.* **2006**, *165*, 100–104.
(26) Stavek, J.; Sipek, M.; Hirasawa, I.; Toyokura, K. Controlled Double-Jet Precipitation of Sparingly Soluble Salts. A Method for the Preparation of High Added Value Materials. *Chem. Mater.* **1992**, *4*, 545–555.
(27) Sardeshpande, M. V.; Kumar, G.; Aditya, T.; Ranade, V. V. Mixing Studies in Unbaffled Stirred Tank Reactor Using Electrical Resistance Tomography. *Flow Meas. Instrum.* **2016**, *47*, 110–121.
(28) Saikali, E.; Rodio, M. G.; Bois, G.; Bieder, U.; Leterrier, N.; Bertrand, M.; Dolias, Y. Validation of the Hydrodynamics in a Turbulent Un-Baffled Stirred Tank: A Necessity for Vortex-Reactor Precipitation Studies. *Chem. Eng. Sci.* **2020**, *214*, No. 115426.
(29) Scargiali, F.; Tamburini, A.; Caputo, G.; Micale, G. On the Assessment of Power Consumption and Critical Impeller Speed in Vortexing Unbaffled Stirred Tanks. *Chem. Eng. Res. Des.* **2017**, *123*, 99–110.
(30) Busciglio, A.; Grisafi, F.; Scargiali, F.; Brucato, A. Mixing Dynamics in Uncovered Unbaffled Stirred Tanks. *Chem. Eng. J.* **2014**, *254*, 210–219.
(31) McCabe, W. L.; Smith, J. C.; Harriott, P. *Unit Operations of Chemical Engineering*, 5th ed.; McGraw-Hill: New York, 1993.
(32) Nichols, G.; Byard, S.; Bloxham, M. J.; Botterill, J.; Dawson, N. J.; Dennis, A.; Diart, V.; North, N. C.; Sherwood, J. D. A Review of the Terms Agglomerate and Aggregate with a Recommendation for Nomenclature Used in Powder and Particle Characterization. *J. Pharm. Sci.* **2002**, *91*, 2103–2109.
(33) Bromley, L. A. Thermodynamic Properties of Strong Electrolytes in Aqueous Solutions. *AIChE J.* **1973**, *19*, 313–320.
(34) Karpiński, P. H.; Bałdyga, J. Precipitation Processes. In *Handbook of Industrial Crystallization*; Myerson, A. S.; Erdemir, D.; Lee, A. Y., Eds.; Cambridge University Press, 2019; pp 216–265.
(35) Parks, G. A. The Isoelectric Points of Solid Oxides, Solid Hydroxides, and Aqueous Hydroxo Complex Systems. *Chem. Rev.* **1965**, *65*, 177–198.
(36) Phillips, V. A.; Kolbe, J. L.; Opperhauser, H. Effect of PH on the Growth of Mg(OH)2 Crystals in an Aqueous Environment at 60 °C. *J. Cryst. Growth* **1977**, *41*, 228–234.

https://doi.org/10.1021/acs.cgd.3c00462
Cryst. Growth Des. XXXX, XXX, XXX–XXX

(37) Stávek, J.; Vondrák, P.; Fořt, I.; Nývlt, J.; Šípek, M. Influence of Hydrodynamic Conditions on the Controlled Double-Jet Precipitation of Silver Halides in Mechanically Agitated Systems. *J. Cryst. Growth* **1990**, *99*, 1098−1103.
(38) Stávek, J.; Hanslík, T.; Zapletal, V. Preparation of High-Temperature Superconductors by Controlled Double-Jet Precipitation. *Mater. Lett.* **1990**, *9*, 90−95.
(39) Mumtaz, H. S.; Hounslow, M. J. Aggregation during Precipitation from Solution: An Experimental Investigation Using Poiseuille Flow. *Chem. Eng. Sci.* **2000**, *55*, 5671.
(40) Xu, C.-h.; Liu, D.; Chen, W. Effects of Operating Variables and Additive on the Induction Period of MgSO4−NaOH System. *J. Cryst. Growth* **2008**, *310*, 4138−4142.
(41) Gunn, D. J.; Murthy, M. S. Kinetics and Mechanisms of Precipitations. *Chem. Eng. Sci.* **1972**, *27*, 1293−1313.

https://doi.org/10.1021/acs.cgd.3c00462
Cryst. Growth Des. XXXX, XXX, XXX−XXX